Analysis of the Impingement of Condensed Rocket Exhaust Products Upon Proximate Space Vehicles

25 p

by

J. R. Wrobel

Abstract

NASA CR 53899

In order to make engineering estimates of the momentum flux and resultant impingement damage to adjacent spacecraft during propulsive maneuvers in space, the size and distribution of condensed vapor constituents of the rocket exhaust are investigated. An analysis of the nucleation, growth and subsequent trajectories of the condensate droplets is presented. The dew points of the constituents of a multicomponent ideal vapor are determined from the Clapeyron relation of reversible thermodynamics. The consequences of a transitory supersaturated vapor state are explored. The growth rate of the condensate droplets is predicted from a kinetic theory model appropriate to the typically rarified flows. The trajectories of the particles are estimated from ideal flow prediction for the purpose of determining the particle flux, the momentum flux, and the energy flux present in the regions remote from rocket nozzles. The time integrated values of these parameters are determined in order to evaluate the cumulative influence of the stream upon an approaching spacecraft. Sample calculations are presented to illustrate the magnitude of these interactions. It is noted that for readily condensible exhausts such as those containing metallic oxides the particle impingement can dictate definite constraints upon the mission profile.

Development Engineer
Liquid Propulsion Section
Jet Propulsion Laboratory
California Institute of Technology
Pasadena, California

Table of Nomenclature

d	condensed particle diameter
h_{fg}	heat of vaporization
I_s	specific impulse
M	mach number
m	molecular weight
N	average number of molecules per particle
n	molecular density
N_o	Avagadro's number
p	pressure
p_v	vapor pressure
R	universal gas constant
r_o	distance between source and target at rocket ignition
r_n	throat radius of the nozzle
s	vapor pressure at condensation $\div$ equilibrium vapor pressure at condensation temperature
T	thermodynamic temperature
t	time
V	velocity of exhausting products
ΔV	rocket velocity increment
w	mass of particulate matter in the exhaust products
x	mole fraction (partial pressure ratio)
θ_d	apex half angle of cone containing particles of diameter d
ϑ_g	apex half angle of gaseous products flow
ϵ_n	apex half angle of rocket nozzle
ρ	mass density
ω	collision frequency
σ	molecular diameter
γ	specific heat ratio

[redacted]

The goal of this investigation is to predict the approximate size and spatial distribution of condensed combustion products in the rarified region of the exhaust of a rocket in space. Condensate particles, moving with velocities on the order of 3000 m/sec relative to the target could, upon impingement, impair the operation of sensitive spacecraft components. In addition to the gross effect of generating tumbling forces, particle pitting of, or adherence to, such surfaces could cause the diffusion of stray light into optical systems or the disruption of the thermal radiation balance from coated surfaces. The exact solution of the particle size and distribution problem is complicated by several effects, most notably those of non-equilibrium thermodynamic behavior and two phase flow dynamics. The study presented does not attempt to delve into these in great detail. The intention was to evolve a simple parametric result useful in making quantitative estimates for mission profile planning and damage evaluation. Several pertinent references, noted at the conclusion of this report, can provide more detailed information on nucleation and associated condensation phenomenon. Several examples are presented to illustrate the application of the guidelines that are established by the approximate survey.

The physical model of the working fluid that is selected for study may be described as follows: The gaseous rocket exhaust products are comprised of perfect vapors, which respectively have constant specific heats and obey the gas law

$$p_i = \rho_i \frac{RT}{m_i}$$

The condensed phases are assumed to be quite dense with respect to their vapors, and exhibit a constant heat of vaporization. This permits the use of the simplified form of the Clausius-Clapeyron relation for the variation

of vapor pressure with temperature in equilibrium, and for infinite surfaces, i.e.,

$$\frac{d(\ln p_{vi})}{d(\ln T)} = \frac{h_{fgi}\, m_i}{RT}$$

The expansion of the vapors from the reservoir or combustion chamber is assumed to occur isentropically, and the local properties of the stream are approximated by the one dimensional gas-dynamic relations

$$\frac{p}{p_t} = \left(1 + \frac{\gamma-1}{2} M^2\right)^{-\gamma/\gamma-1}$$

$$\frac{T}{T_t} = \left(1 + \frac{\gamma-1}{2} M^2\right)^{-1}$$

As regards condensation, Wegener (1) and others have illustrated that the vapor pressure decreases more rapidly with decreasing temperature than does the static pressure in typical isentropic nozzle flows. The ratio can be shown to be

$$\frac{\left(\frac{dp_{vi}}{dT}\right)}{\left(\frac{dp_i}{dT}\right)} = \frac{h_{fgi}\, m_i}{RT}\left(\frac{\gamma-1}{\gamma}\right)$$

Therefore, at some point in the expansion, saturation will occur, i.e., $\frac{p_i}{p_{vi}} = 1$ In general, condensation will not occur precisely at the (equilibrium) saturation point, but a finite super-saturation will be exhibited. This phenomenon can be related to the influence of capillarity and the presence of suitable nucleation sites for condensation to begin, cf (2). In the present model, the ratio of the static pressure at condensation to the equilibrium vapor pressure is designated as $\underline{s}$ $\left(S = \frac{p_{ci}}{p_{vi}}\right)$ and is treated parametrically to determine the relative importance of supersaturation in the problem under study. Combining the gas law, the vapor pressure dependence and the isentropic flow functions results in an implicit solution for the Mach number of the flow at the initiation of condensation

$$\frac{m_i h_{fgi}}{RT_t}\left(\frac{\gamma-1}{2}\right)M_{ci}^2 - \frac{\gamma}{\gamma-1}\ln\left(1+\frac{\gamma-1}{2}M_{ci}^2\right) = \frac{m_i h_{fgi}}{RT_t}\left[\frac{T_t}{T_o}-1\right] + \ln a_i - \ln x_i - \ln\frac{P_t}{P_o}$$

The effective stagnation temperature for each of the constituent vapors depends upon the sequence of condensation, for the energy release upon phase change of one constituent results in an attendant rise in stagnation enthalpy of the remaining vapors, and the adiabatic relations no longer apply. A mixture of vapors will exhibit sequential condensation, with the readily condensible constituents providing nuclei for the more volatile constituents. The treatment of an expanding flow with non-equilibrium energy release is beyond the scope of this investigation. An estimate of the dew point of the vapors can be made if it is assumed that the heat release of the initially condensing vapors has a negligible effect upon the flow as predicted by the isentropic relations. In this way, a limiting bound is established. Thermal choking, i.e., the reduction of the local Mach number to unity due to energy release is not a significant problem at the typically high Mach numbers experienced at the dew point of the prevailing exhaust products.

The Mach number at condensation for several candidate spacecraft propulsion systems were determined from the solution of the preceeding implicit function. Physical property data extracted from (3) are presented in Table (1). The chemical propellant systems investigated include two mono-propellants, a liquid bi-propellant combination and two composite solid propellants. Specifically, these are hydrazine, hydrogen peroxide, nitrogen tetroxide hydrazine, ammonium perchorate (AP)/hydrocarbon (HC), and ammonium perchlorate/hydrocarbon/aluminum. The effective stagnation temperature, products composition, and specific heat ratio for these chemical systems are presented

in Table (2). The heats of vaporization and boiling points of the products, presented in Table (1), are evaluated at one atmosphere pressure.

The Mach number of the stream at condensation has been computed for the first two constituents to "freeze" for each of the candidate systems with equilibrium condensation, and with finite supersaturation. As was mentioned, the estimate of the condensation point for the second vapor is quite approximate. The results of this calculation are presented in Table (3).

It is apparent that low stagnation enthalpy monopropellant systems (hydrazine and hydrogen peroxide) show a greater tendency to exhaust condensation than do the others. The influence of super-saturation will become more apparent in the particle size discussion which follows. The case of the aluminized solid propellant system is deferred to a subsequent section because of the non-typical nature of the droplet condensation.

At the low pressures and temperatures associated with the condensation of non-metallic rocket exhaust products, the condensation phenomenon can no longer be considered to be a spontaneous process. The collision rate of vapor molecules becomes quite small compared with that at standard conditions. Therefore the growth rate of the condensate particles is limited. In the following, an attempt is made to estimate the size of the particles, as predicted from the kinetic theory. Intrinsic in this method is the assumption of nearly Maxwellian molecular velocity distributions. Again, the goal is to investigate the phenomenon parametrically. The binary collision frequency of heterogeneous spherical molecules, as presented in (4), is, per unit of volume and time.

$$\omega_{12} = \frac{n_1 n_2}{2} \left(\sigma_1 + \sigma_2\right)^2 \left(\frac{2\pi RT\,(m_1 + m_2)}{m_1 m_2}\right)^{\frac{1}{2}}$$

If it is assumed that each binary collision of vapor and condensate adds to the size of the droplet and that higher order collisions, including those among droplets can be neglected, the particle growth rate becomes

$$\frac{dN_i}{dt} = N_o \frac{\rho_i}{2} \sigma_i^2 N_i^{2/3} \left(\frac{2\pi RT}{m_i} \right)^{\frac{1}{2}}$$

This assumes that the effect of vapor depletion can be neglected, at least to obtain an upper bound of the particle size. If the average flow velocity of the stream is assumed to be constant, as is nearly the case for high Mach number flow, and that the gas density in the condensation region decays as in conical source flow, the integral becomes, in Mach number coordinates

$$N^{\frac{1}{3}} = \frac{N_o \chi_i p_t \sigma_i^2}{3\sqrt{2} R T_t V} \left(\frac{\pi R T_t}{m_i} \right)^{\frac{1}{2}} \frac{r_n}{\tan \theta_n} \left(\frac{\gamma+1}{2} \right)^{-\frac{\gamma+1}{4(\gamma-1)}} \frac{1}{M_{c_i}^{r_2}} \left(1 + \frac{\gamma-1}{2} M_{c_i}^2 \right)^{-\frac{1}{4}\frac{\gamma+1}{\gamma-1}}$$

From this, the influence of the parameters of the problem become more obvious. Using the information from Table (3) for the condensation Mach number, the average number of molecules per droplet was evaluated for several of the examples. It must be assumed that the particles can persist in space, since the surface tension in small radius of curvature particles is appreciable.

For the hydrogen peroxide system, the water droplets could contain approximately 10^5 molecules if equilibrium condensation occurred, but only approximately 5×10^3 molecules if the assumed supersaturation occurs. Optical instruments designed for the visible spectrum will be essentially unaffected by such particles, since the typical sub-micron size is smaller than the wave-length of the radiation of interest. Instruments designed for ultra-violet discrimination could be affected, if exposed to the stream. The largest particles estimated for the propellant systems of interest were approximately 0.15 μ.

Since these exhaust products condense late in the expansion process,

where the velocity direction and magnitude are approaching the limiting case of infinite expansion, the particles may be assumed to be distributed in a pattern similar to that of the gaseous exhaust plume. For the larger particles, experienced in metallized propellant combustion, this is not the case and will be discussed subsequently.

The exhaust plume of an ideal non-condensing gas expanding into a vacuum can be determined from the solution of the hyperbolic equations of supersonic flow referred to as the "method of characteristics" solution in (5). Examination of many such solutions for the region far from the throat indicates that the mass flux along the centerline decays as an inverse square function of the distance from a virtual source near the throat. Experimental evidence confirms this behavior, as indicated in (6). The mass flux variation as a function of conical apex angle for axisymmetric flows has been examined to determine the trend for particle flux estimates. A sound approximation to the angular variation has been found to be

$$\frac{(\text{mass flux})_\theta}{(\text{mass flux})_{Axis}} = 0.5\left[1 + \cos\frac{\pi\theta}{\theta_m}\right]$$

In this approximating function, θ_m is the limiting turning angle for the ideal gas flow expanding from the nozzle exit Mach number(M_e) to infinite Mach number. This angle is defined to be

$$\theta_m = \theta_n + \left(\sqrt{\frac{\gamma+1}{\gamma-1}} - 1\right)\frac{\pi}{2} - \sqrt{\frac{\gamma+1}{\gamma-1}}\tan^{-1}\sqrt{\frac{\gamma-1}{\gamma+1}(M_e^2-1)} + \tan^{-1}\sqrt{M_e^2-1}$$

For the sub-micron size condensate particles, the particle distribution has been assumed to follow the gas flux distribution.

The case of the aluminized solid propellant is studied separately because of the atypical phase transition behavior which occurs. The stable aluminum

oxide condensate is formed by the reaction of gaseous sub-oxides, and not from a vapor phase per se. Apparently the transition occurs almost entirely in the combustion chamber and is virtually complete before entering the expansion region cf (7). A considerable amount of experimental work has been conducted i.e. (8), to determine the size of these condensate droplets, although there is apparently no satisfactory method of analytically predicting the size. No such attempt was made in the present investigation, rather the available experimental data was relied upon. See figure (1) for representative aluminum oxide particle size data.

The analysis of (9) was applied to determine the distribution of the various particles in the exhaust. The region of interest was that outside the nozzle proper, and the influence of two phase flow upon the specific impulse delivered by the nozzle was not considered. The density of particles per unit volume and the particle mass flux was computed for a typical space propulsion system configuration. The particle density at the axis of symmetry of the jet is predicted to decay as the inverse square of the distance along the axis, as presented in figure (2). The distinguishing feature of the calculation is the prediction that the particles of a given size are contained in a cone of expansion whose apex angle is a function of the particle size. In general, the greater the particle size, the smaller the apex angle. This is illustrated schematically in fig (3). The conical angle as a function of particle size is presented in fig (4). The distribution of the particles within the cone is not uniform, but does not vary by a large amount, c.f. figure (5).

The mass flux of particles, of a given size, at some distance from the source can be simply estimated, if it is assumed that the non-uniformity of particle distribution over the containing cone for the specific size is negligible. Assuming an average acceleration over the rocket burning time, the

total particulate mass of specified size intercepting unit transverse area initially at range r_o is given by

$$\frac{mass}{AREA} = \frac{w}{2\pi(1-\cos\theta)r_o^2}\,\frac{1}{2}\left[\frac{\tan^{-1}\sqrt{\frac{\Delta V t_b}{2r_o}}}{\sqrt{\frac{\Delta V t_b}{2r_o}}} + \frac{1}{1+\frac{\Delta V t_b}{2r_o}}\right]$$

for departing spacecraft, and

$$\frac{mass}{AREA} = \frac{w}{2\pi(1-\cos\theta)r_o^2}\,\frac{1}{2}\left[\frac{1}{2}\frac{\ln\frac{\left(1+\sqrt{\frac{\Delta V t_b}{2r_o}}\right)}{\left(1-\sqrt{\frac{\Delta V t_b}{2r_o}}\right)}}{\sqrt{\frac{\Delta V t_b}{2r_o}}} + \frac{1}{1+\frac{\Delta V t_b}{2r_o}}\right]$$

for rendezvousing spacecraft. The first term is appropriate to impulsive burning, the second is the attenuation coefficient appropriate to finite burning time of the rocket. This attenuation coefficient is plotted in figure (6).

It is worthwhile to note that for the analogous case of purely gaseous expansion, the mass flux of gas at a given range may be considerably less than that of the particles even though there are proportionately more gaseous products than condensed, i.e., along the axis

$$\frac{\left(\frac{mass}{AREA}\right)_{GAS}}{\left(\frac{mass}{AREA}\right)_{COND.}} = \frac{\text{mass of gas}}{\text{mass of condensate}}\,\frac{1-\cos\theta_{cond.}}{1-\cos\theta_{gas}}$$

The appropriate gaseous expansion angle (θ_g) has been estimated from gas-dynamic theory (Prandtl-Meyer expansion). The gas mass flux may be as small as 1% of the particle flux for micron-size aluminized exhaust products far from the source. This is due to the focusing effect noted for the two-phase system.

The preceeding results for particle mass flux may be adapted to predict the number of particles striking a unit transverse area or to the fraction of the target area covered by the impinging particles, assuming non-overlapping

impacts. These are, for the case of impulsive burning.

$$\frac{\text{number}}{\text{area}} = \frac{3w}{\pi^2(1-\cos\theta_d)r_o^2\rho_p d^3}$$

$$\text{fraction of transverse area covered} = \frac{3w}{4\pi r_o^2(1-\cos\theta_d)\rho_p d}$$

Adjustment of these values for non-impulsive burning may be made by applying the attenuation coefficient of fig. (6).

The velocity with which the particles travel with respect to the source is difficult to predict precisely. A characteristic velocity to use as an estimate is that of the idealized exhaust, i.e.

$$V = I_s$$

From this, it is possible to determine the momentum and energy per particle. These are respectively

$$\text{momentum} = \rho_p \frac{\pi}{6} d^3 I_s$$

$$\text{kinetic energy} = \rho_p \frac{\pi}{12} d^3 I_s^2$$

The momentum, and energy associated with aluminum oxide particles exhausting from a rocket with specific impulse of 300 sec (V = 2958 m/sec) are presented in figures (7) and (8) respectively.

Many particle impact studies have been conducted to study the cratering effect of micrometeorite impact. A considerable amount of this work has been in the velocity range of typical rocket exhausts. Figure (9) presents an example of some typical data. It has been observed that craters in ductile materials resulting from the impact of ductile particles are proportional to the size of the particle and a function of the impact velocity. The impact of brittle tungsten carbide particles upon ductile materials appears to follow

the data for ductile particles. For impact velocities of 2,000 to 4,000 m/sec, the ratio of the crater diameter to the particle diameter will be approximately three. Using this value, the fraction of the transverse area covered by craters, is presented in figure (10) as a function of range for aluminum oxide particles emanating from a motor containing 50 K.g. of propellant.

It is evident that there is a considerable hazard to sensitive spacecraft systems from the aluminum oxide particles of multi-micron size. However, the hazard diminishes drastically if the target area can be displaced from the stream axis by only a few degrees. If propellant systems containing readily condensible products are to be employed for spacecraft propulsive maneuvers the vehicle configuration and/or the mission execution and maneuvering sequence will have to be appropriately biased. There does not appear to be a significant problem resulting from the impingement of the products of non-metallized propellants, provided that the full adiabatic flame temperature is developed. In the intermittent operation of small spacecraft motors, thermal transients can be severe, and therefore a considerably greater degree of condensation may occur in such operations.

References:

9. J. Kliegel, Gas Particle Nozzle Flows, Ninth Symposium on Combustion, Academic Press, N. Y. 1963

8. R. Sehgal, Experimental Investigation of a Gas Particle System Ninth Symposium on Combustion, Academic Press, N. Y., 1963

1. P. Wegener, Condensation Phenomenon in Nozzles AIAA Heterogeneous Combustion Conference, 12/63 AIAA Preprint 63-509

2. J. Keenan "Thermodynamics" J. Wiley & Sons N. Y. 1941

4. S. Chapman & T. Cowling "The Mathematical Theory of Non Uniform Gases" Cambridge University Press London 1960

3. Handbook of Chemistry and Physics C. Hodgman, ed. 43rd Edition Chemical Rubber Publishing Co. Cleveland, Ohio 1961

5. H. W. Liepmann & A. Roshko "Elements of Gasdynamics" J. Wiley and Sons New York 1957

6. W. Latto, Jr. & L. Stitt, Highly Underexpanded Exhaust Jet Against Adjacent Surfaces, Journal of Aeronautics and Aerospace Engineering pp. 107-10 (date unknown)

7. H. Chueng and N. Cohen "On the Performance of Solid Propellants Containing Metal Additives" AIAA Solid Propellant Rocket Conference - January 1964.

Table 1

Physical Properties of Selected Exhaust Products

Ref (3)

Physical Property	Constituent							
	H_2O	HCl	CO_2	CO	NH_3	N_2	O_2	H_2
Molecular Weight (gm/gm mol)	18	36.5	44.0	28	17.0	28.0	32.0	2
Heat of Vaporization (cal/gm)	540	98.7	87.2	50.4	327	47.6	50.9	108
Standard Boiling Point (^{o}C)	100	-83.7	-78.5	-190	-33	-196	-183	-253

Table 2

Combustion Products and Flame Temperature of Candidate Propellants

Property	Propellant System				
	N_2H_4	90% H_2O_2	N_2O_4/N_2H_4 O/F=1.2	AP/HC	AP/HC/ 16% AL
Stagnation Temperature (^oC)	1037	750	2788	2650	3185
Effective Specific Heat Ratio*	1.38	1.35	1.29	1.35	1.23
Mole Fraction of Gaseous Constituents					
H_2O	----	.708	.489	.135	.124
HCl	----	----	----	.156	.159
CO_2	----	----	----	.204	.040
CO	----	----	----	.091	.242
NH_3	.330	----	----	----	----
H_2	.390	----	.096	.301	.367
N_2	.280	----	.415	.079	.078
O_2	----	.292	----	----	----

*Evaluated at Area Ratio of 40:1

Table 3

Mach Number of Vapor Condensation

P_t = 10 atm

Propellant System	Condensation Mach No.			
	S=1		S=4	
	a	b	a	b
N_2H_4	NH_3@ 6.4	N_2@ 14.5	NH_3@ 6.8	N_2@ 15.1
90% H_2O_2	H_2O@ 3.6	O_2@ 11.9	H_2O@ 3.9	O_2@ 12.4
N_2O_4/N_2H_4	H_2O@ 9.7	N_2@ 30.5	H_2O@ 10.1	N_2@ 31.2
AP/HC	H_2O@ 8.0	HCl@ 19.0	H_2O@ 8.4	HCl@ 19.6
AP/HC/16% AL	H_2O@ 13.0	HCl@ 21.1	H_2O@ 13.4	HCl@ 21.5 *

*Excluding Aluminum Oxide

AVERAGE PARTICLE SIZE AS A FUNCTION OF PRESSURE FOR AN ALUMINIZED COMPOSITE SOLID PROPELLANT

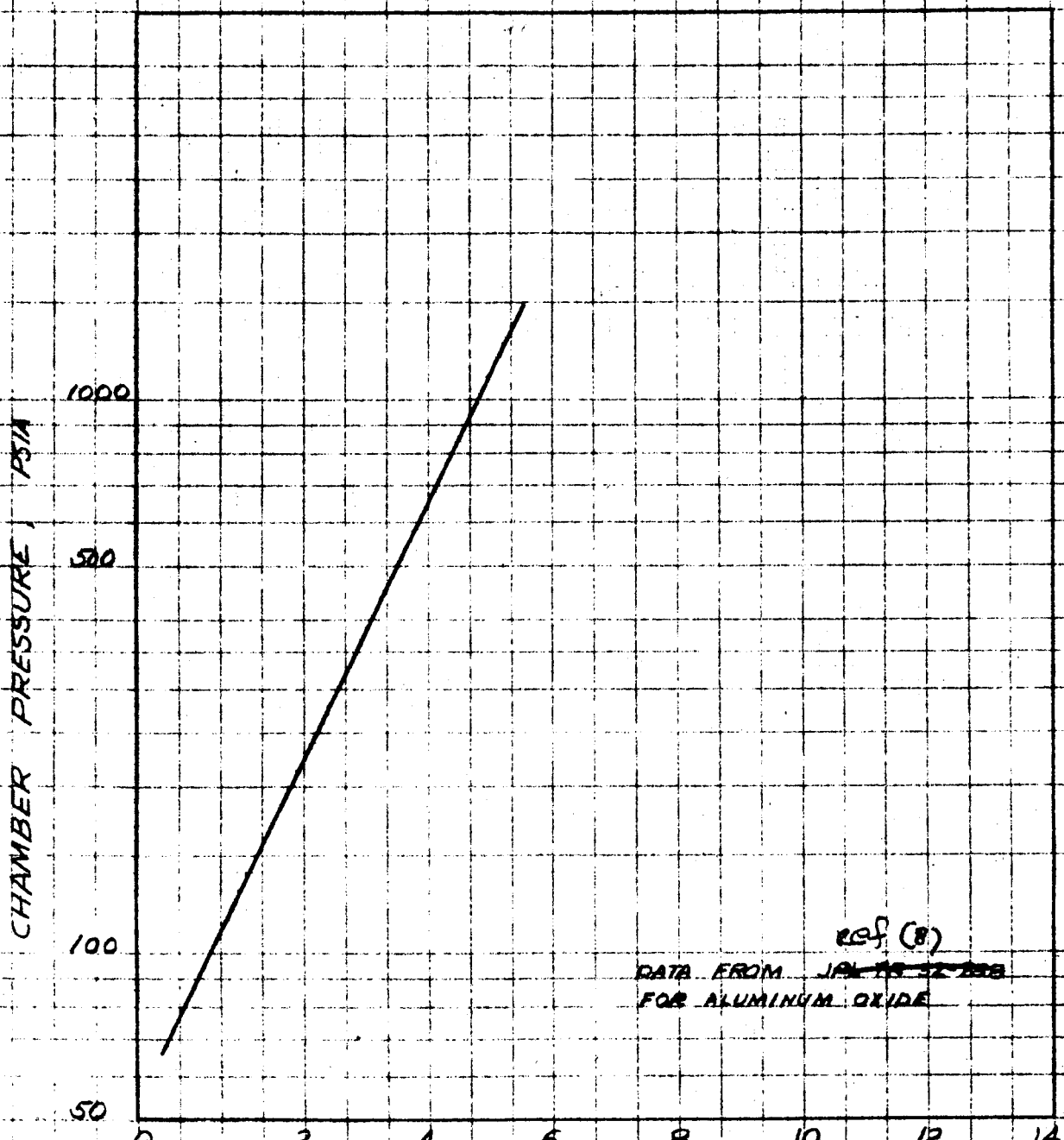

FIGURE 1

~~FIG 1~~

JRW 7/63

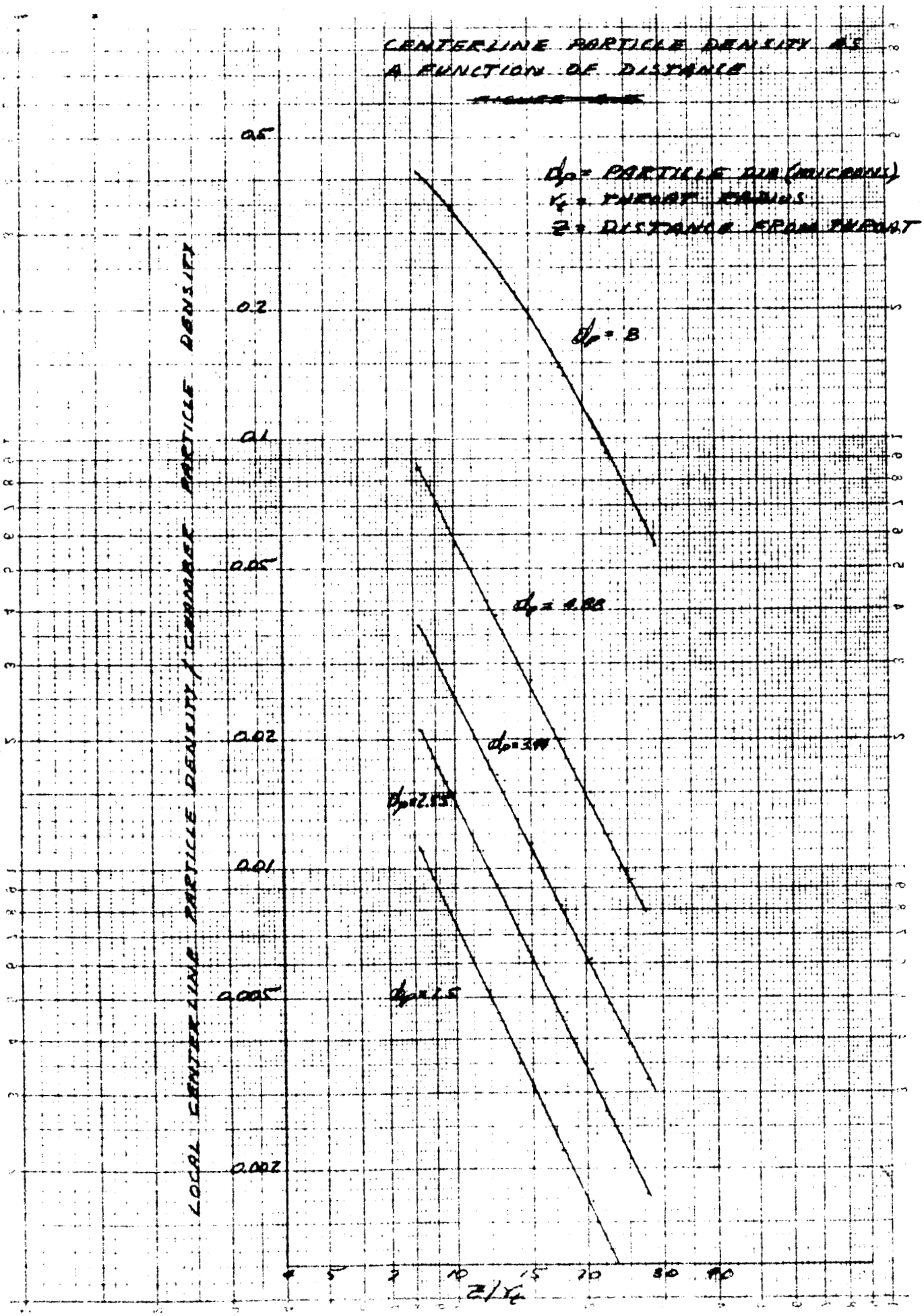
CENTERLINE PARTICLE DENSITY AS A FUNCTION OF DISTANCE
d_o = PARTICLE DIA (MICRONS)
r_t = THROAT RADIUS
z = DISTANCE FROM THROAT
$d_p = 8$
$d_p = 4.88$
$d_p = 3.44$
$d_p = 2.53$
$d_p = 1.5$
LOCAL CENTERLINE PARTICLE DENSITY / CHAMBER PARTICLE DENSITY
0.5
0.2
0.1
0.05
0.02
0.01
0.005
0.002
5
7
10
15
20
30
40
z/r_t

FIGURE 2

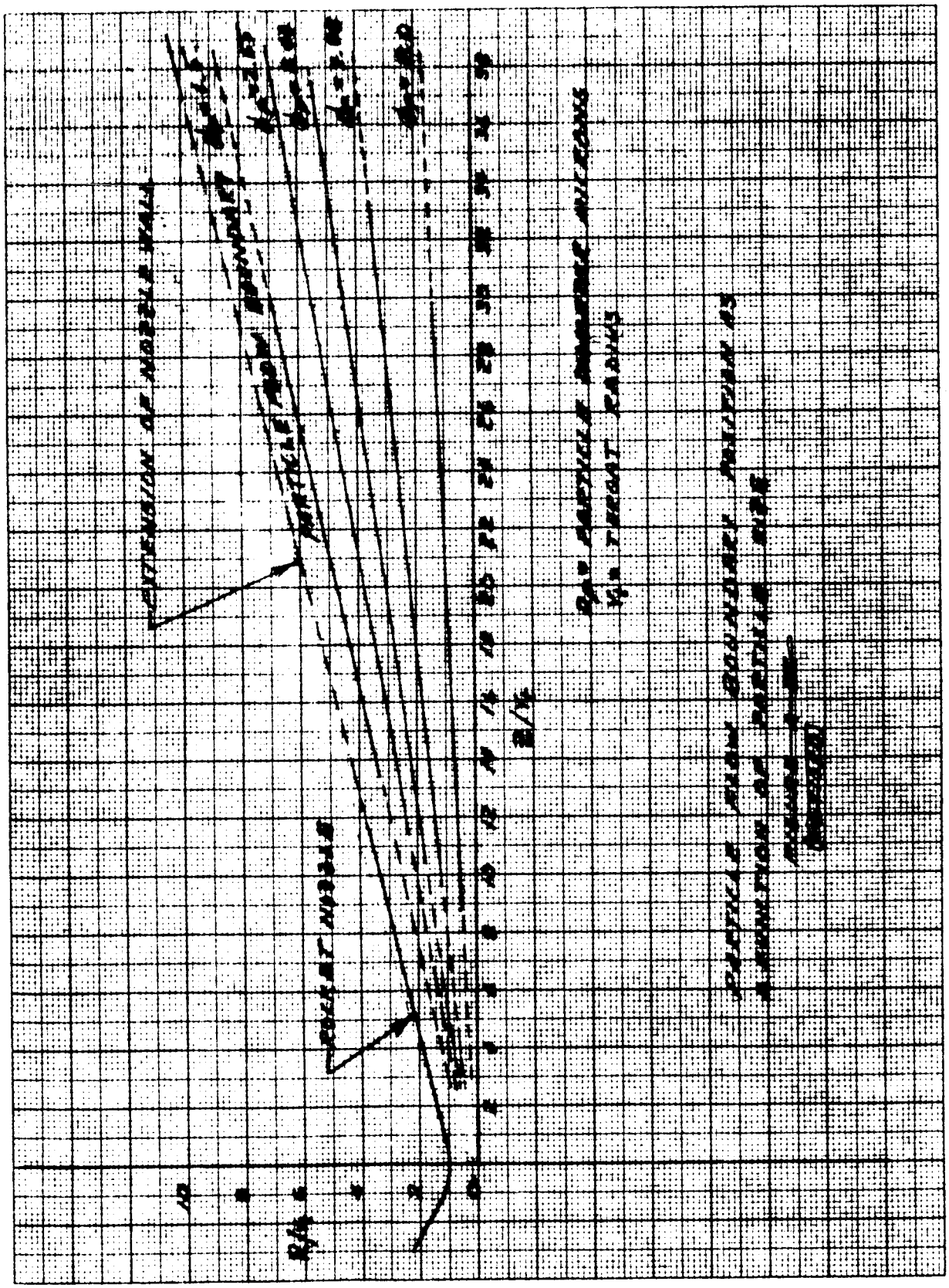

FIGURE 3

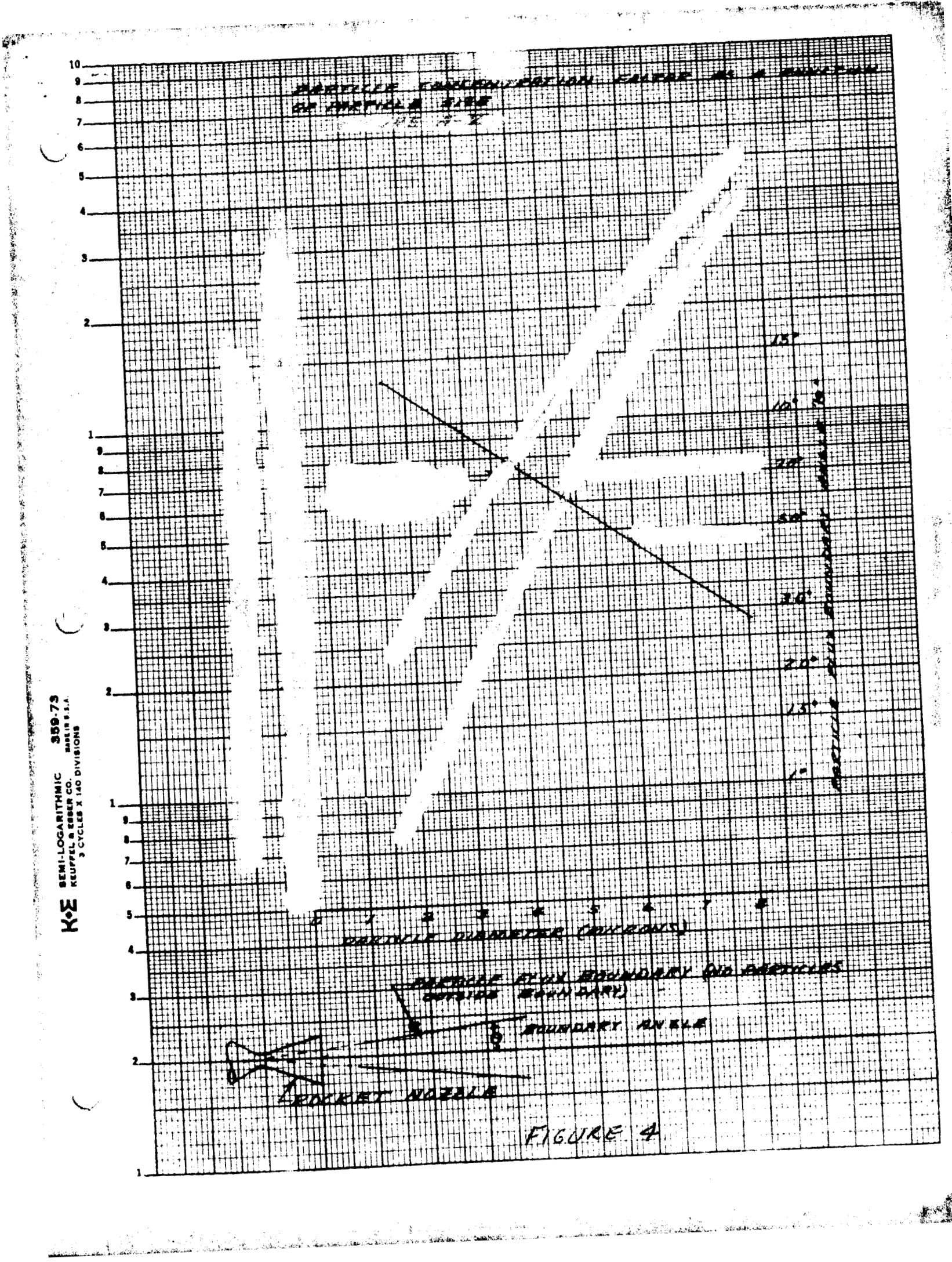
PARTICLE TRAJECTORY FOR ONE PARTICLE SIZE
PARTICLE DIAMETER (MICRONS)
PARTICLE FLOW BOUNDARY FOR PARTICLES OUTSIDE BOUNDARY
BOUNDARY ANGLE
ROCKET NOZZLE
PARTICLE FLOW BOUNDARY ANGLE
SEMI-LOGARITHMIC 359-73
KEUFFEL & ESSER CO.
3 CYCLES X 140 DIVISIONS

FIGURE 4

PARTICLE CONCENTRATION FACTOR AS A FUNCTION OF DISPERSION IN JET PLUME

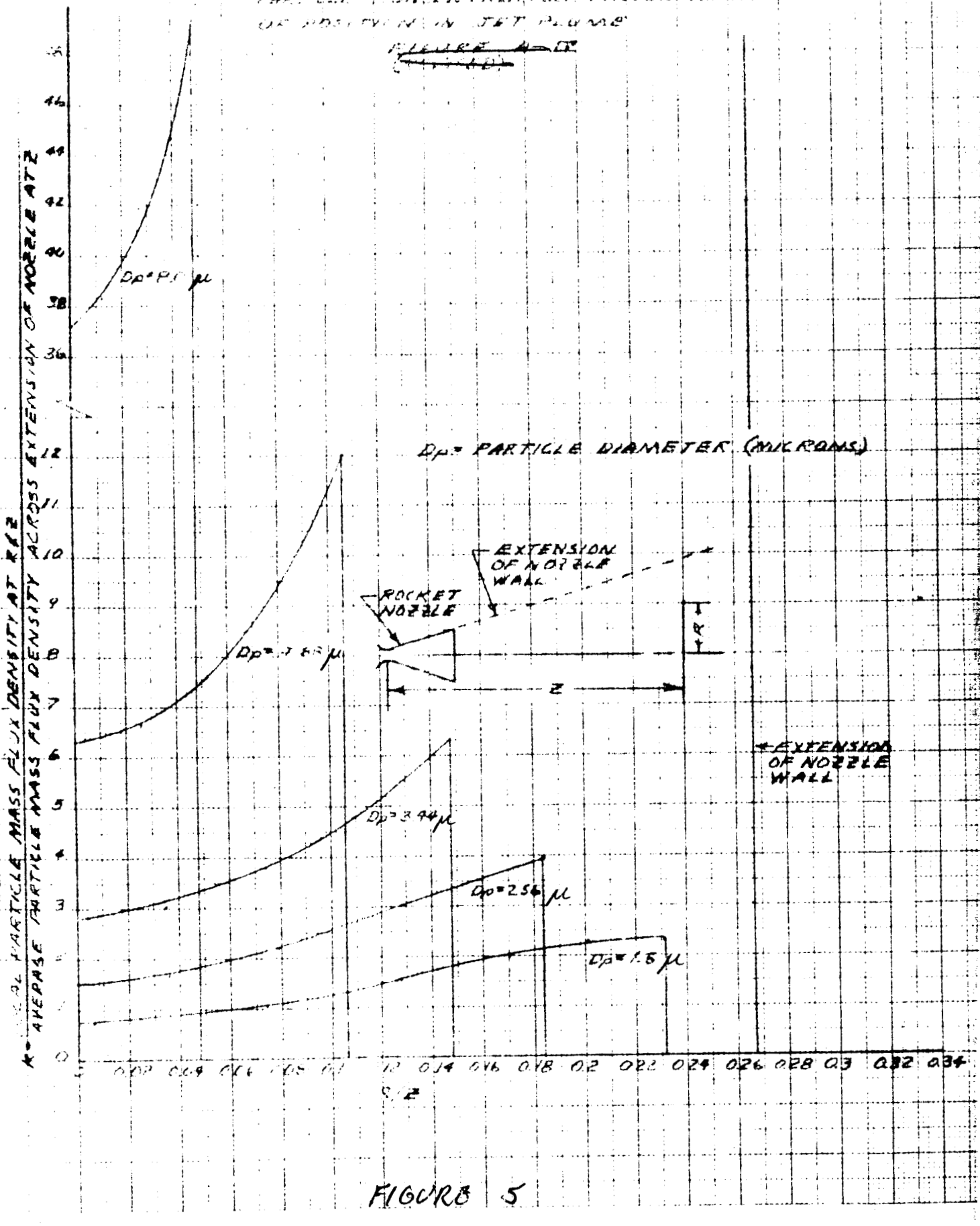

FIGURE 5

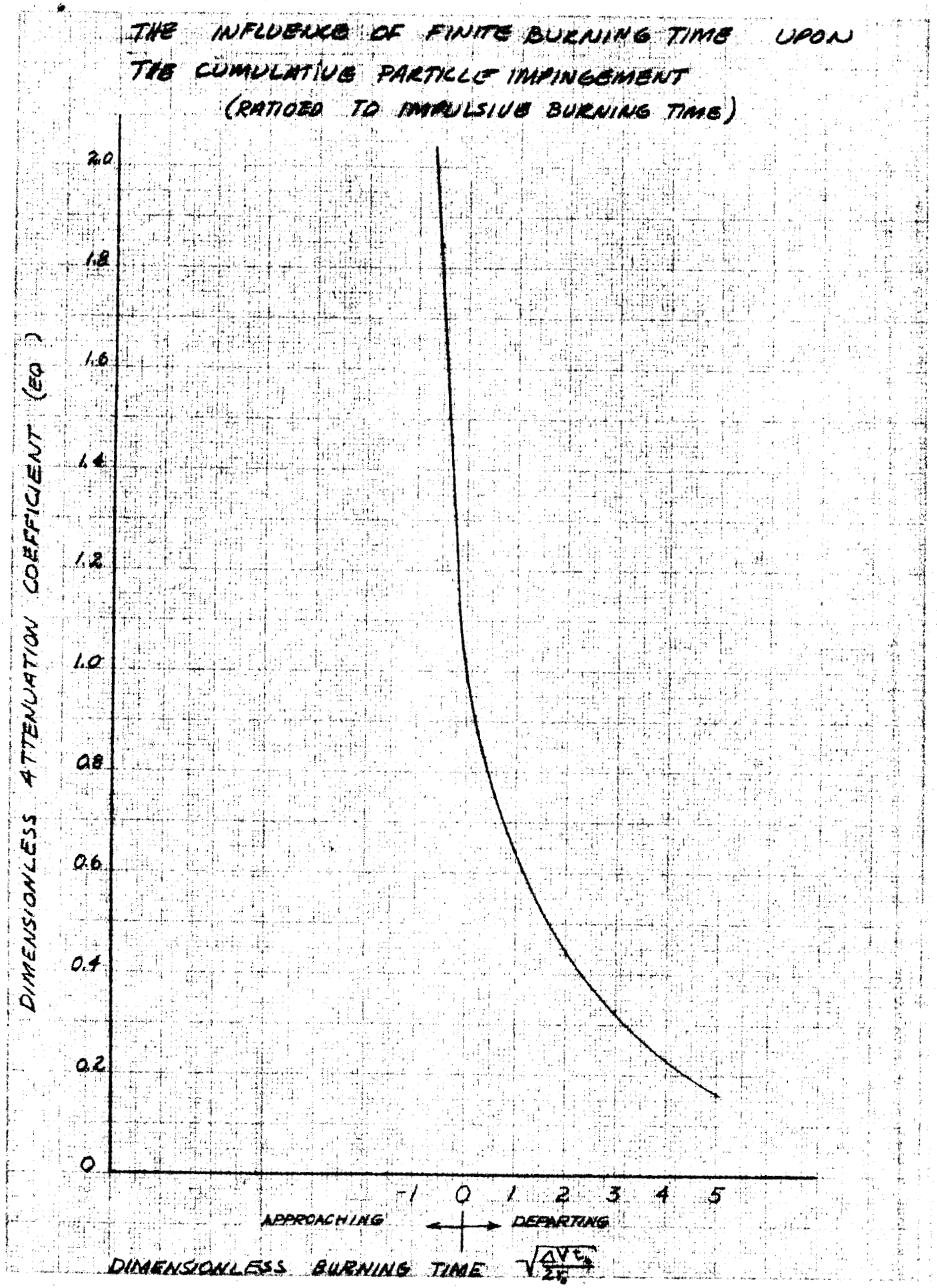
THE INFLUENCE OF FINITE BURNING TIME UPON
THE CUMULATIVE PARTICLE IMPINGEMENT
(RATIOED TO IMPULSIVE BURNING TIME)
DIMENSIONLESS ATTENUATION COEFFICIENT (EQ)
2.0
1.8
1.6
1.4
1.2
1.0
0.8
0.6
0.4
0.2
0
-1
0
1
2
3
4
5
APPROACHING
DEPARTING
DIMENSIONLESS BURNING TIME

FIGURE 6

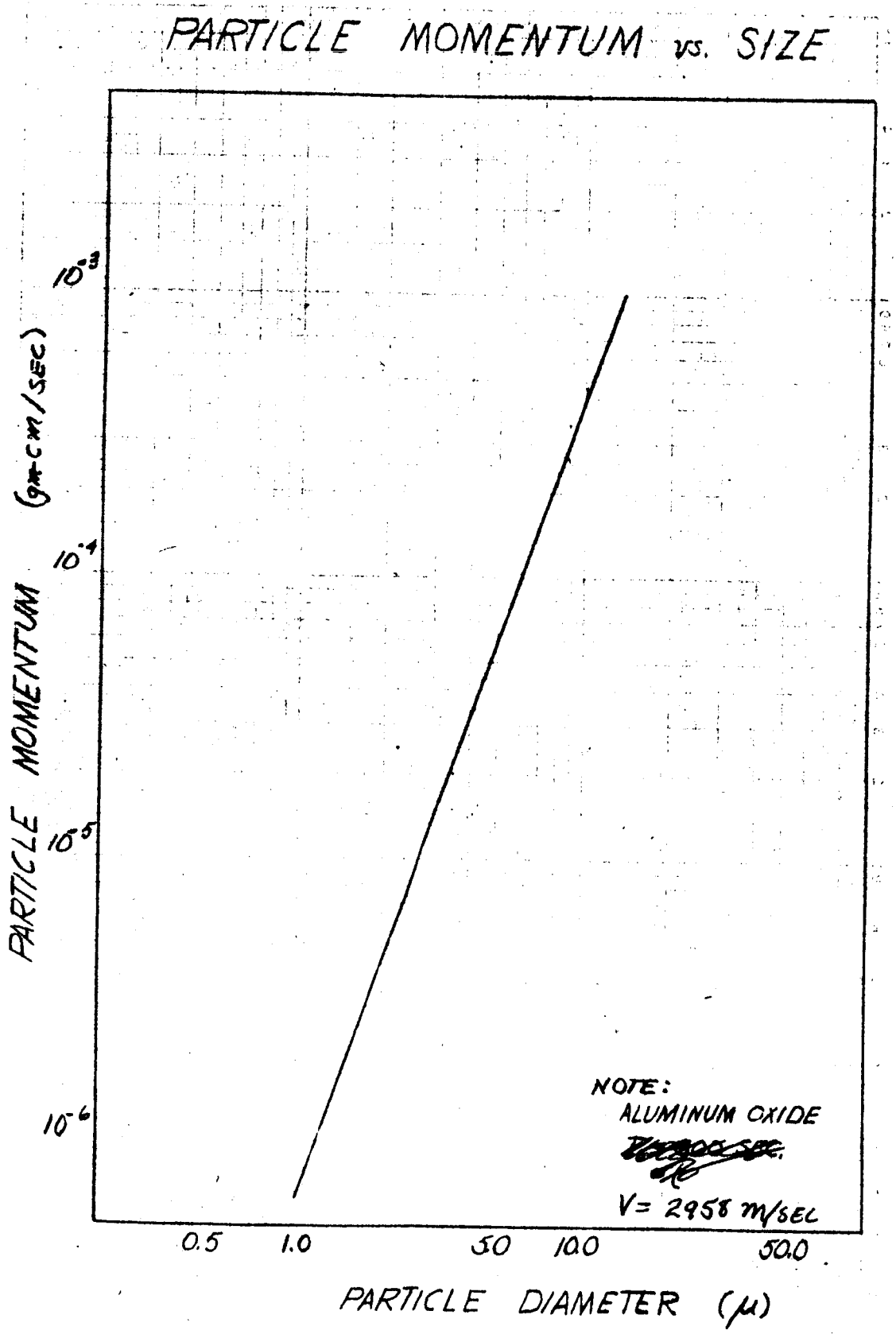
PARTICLE MOMENTUM vs. SIZE
PARTICLE MOMENTUM (gm-cm/sec)
10^{-3}
10^{-4}
10^{-5}
10^{-6}
NOTE:
ALUMINUM OXIDE
V= 2958 m/sec
0.5
1.0
5.0
10.0
50.0
PARTICLE DIAMETER (μ)

FIG. 7

JRW 7/63

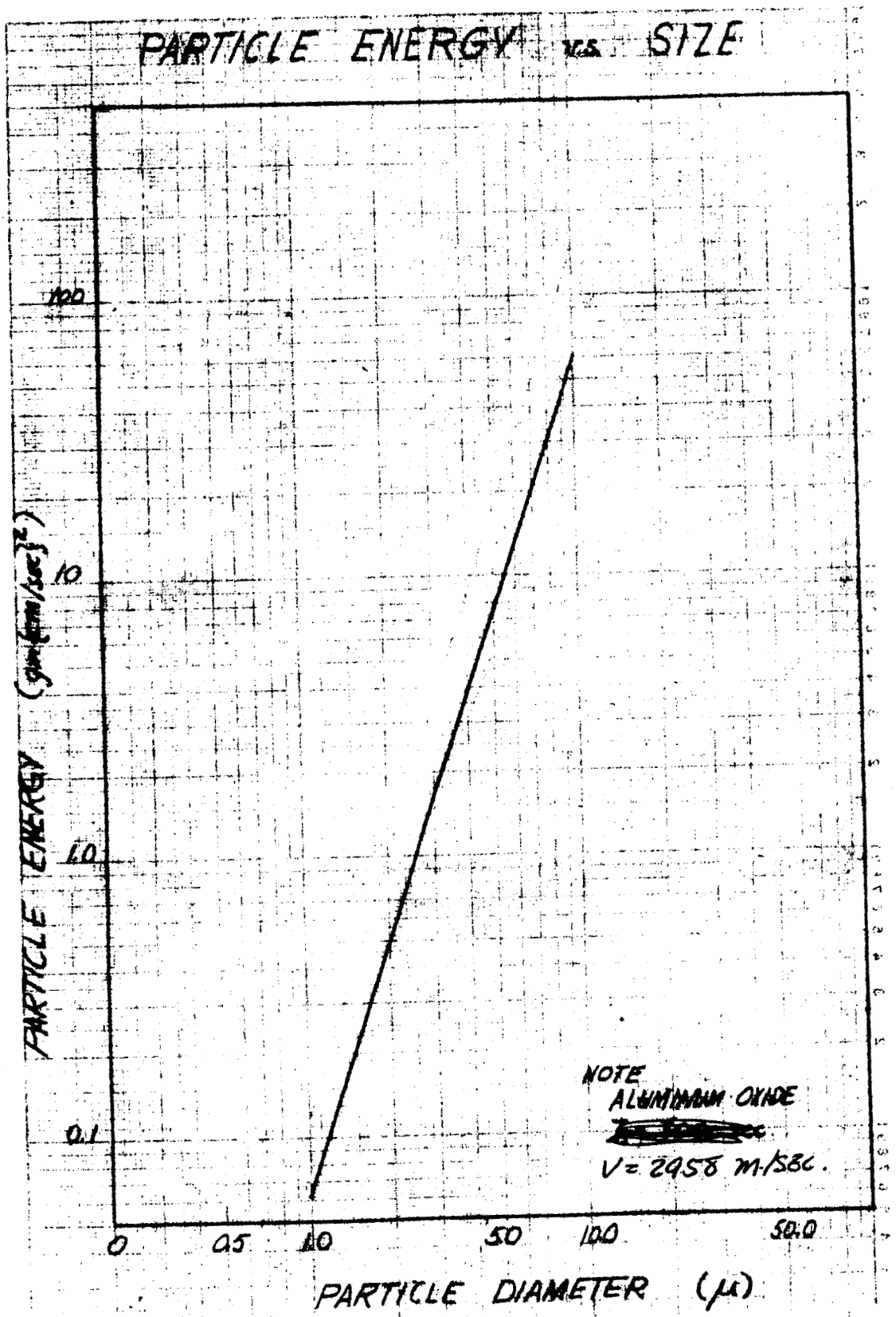
PARTICLE ENERGY vs. SIZE
PARTICLE ENERGY (gm-cm/sec²)
100
10
1.0
0.1
0
.05
.10
.50
1.00
5.00
PARTICLE DIAMETER (μ)
NOTE
ALUMINUM OXIDE
V = 2958 M/SEC.

FIG. 8

JRM 7/63

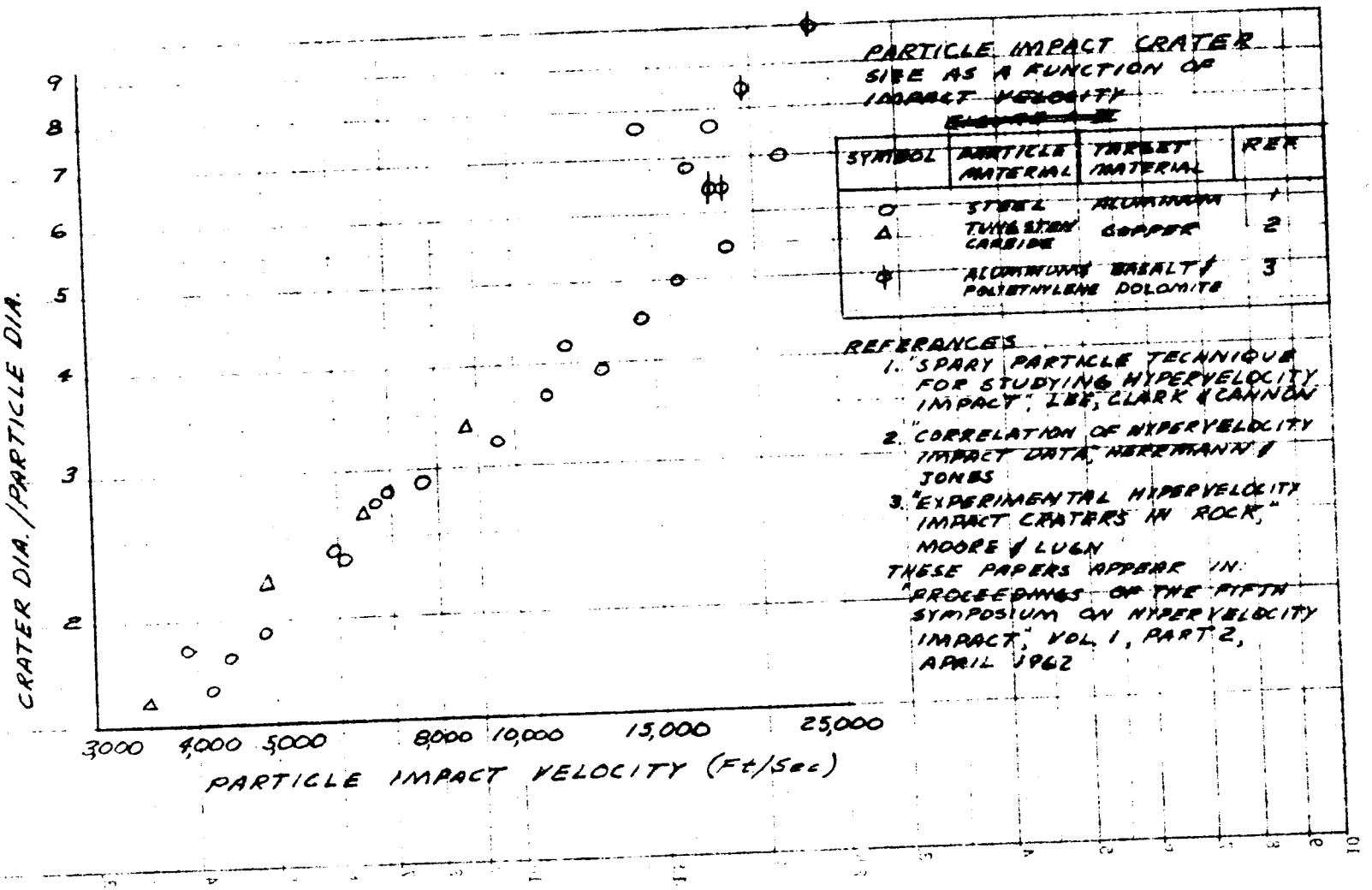
PARTICLE IMPACT CRATER SIZE AS A FUNCTION OF IMPACT VELOCITY
SYMBOL
PARTICLE MATERIAL
TARGET MATERIAL
REF
STEEL
ALUMINUM
1
TUNGSTEN CARBIDE
COPPER
2
ALUMINUM POLYETHYLENE
BASALT & DOLOMITE
3
REFERANCES
1. "SPARY PARTICLE TECHNIQUE FOR STUDYING HYPERVELOCITY IMPACT", LEE, CLARK & CANNON
2. "CORRELATION OF HYPERVELOCITY IMPACT DATA", HERRMANN & JONES
3. "EXPERIMENTAL HYPERVELOCITY IMPACT CRATERS IN ROCK", MOORE & LUGN
THESE PAPERS APPEAR IN "PROCEEDINGS OF THE FIFTH SYMPOSIUM ON HYPERVELOCITY IMPACT", VOL. I, PART 2, APRIL 1962
CRATER DIA./PARTICLE DIA.
9
8
7
6
5
4
3
2
3000
4,000
5000
8,000
10,000
15,000
25,000
PARTICLE IMPACT VELOCITY (Ft/Sec)

FIGURE 9.

CRATER COVERAGE AS A FUNCTION OF RANGE FOR A TYPICAL ALUMINIZED SOLID PROPELLANT

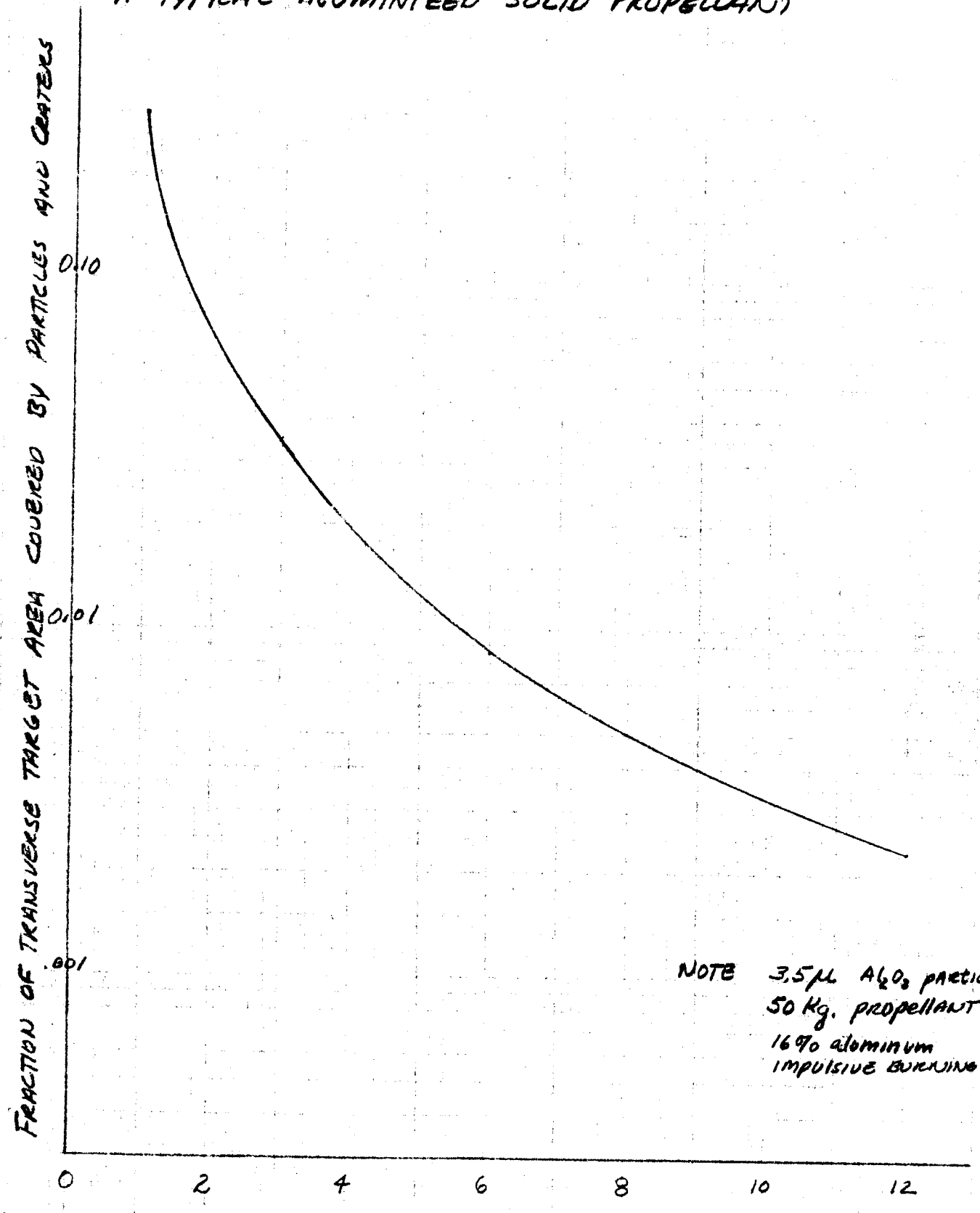

FIG. 10